Geophysical Research Letters

RESEARCH LETTER
10.1029/2022GL100984

Interannual Variability of Near-Inertial Energy in the South China Sea and Western North Pacific

Huaihao Lu[1,2], Zhiwu Chen[1,3], Kang Xu[1,3], Zhiyu Liu[4], Chunzai Wang[1,3,5], Jiexin Xu[1,3], Yankun Gong[1,3], and Shuqun Cai[1,3,5]

[1]State Key Laboratory of Tropical Oceanography, South China Sea Institute of Oceanology, Chinese Academy of Sciences, Guangzhou, China, [2]University of Chinese Academy of Sciences, Beijing, China, [3]Southern Marine Science and Engineering Guangdong Laboratory (Guangzhou), Guangzhou, China, [4]State Key Laboratory of Marine Environmental Science, Department of Physical Oceanography, College of Ocean and Earth Sciences, Xiamen University, Xiamen, China, [5]Institution of South China Sea Ecology and Environmental Engineering, Chinese Academy of Sciences, Guangzhou, China

Key Points:

- Mixed-layer near-inertial energy in the study region correlates negatively with El Niño-Southern Oscillation (ENSO) with a time lag of 5 months
- Summer near-inertial energy is mainly generated by tropical cyclones and correlates positively with ENSO
- Winter near-inertial energy is mainly generated by the winter monsoon and correlates negatively with ENSO

Supporting Information:

Supporting Information may be found in the online version of this article.

Correspondence to:

Z. Chen and S. Cai,
zhiwuchen@scsio.ac.cn;
caisq@scsio.ac.cn

Citation:

Lu, H., Chen, Z., Xu, K., Liu, Z., Wang, C., Xu, J., et al. (2022). Interannual variability of near-inertial energy in the South China Sea and western North Pacific. *Geophysical Research Letters*, *49*, e2022GL100984. https://doi.org/10.1029/2022GL100984

Received 29 AUG 2022
Accepted 8 DEC 2022

Abstract Interannual variability of surface mixed-layer near-inertial energy (NIE, representing the intensity of near-inertial waves) in the South China Sea and western North Pacific (WNP) is investigated using satellite-tracked surface drifter data set. It is found that NIE in the study region correlates negatively with El Niño-Southern Oscillation (ENSO) with a correlation coefficient of $R = -0.44$ and a time lag of 5 months, mainly because the variation of local wind stress lags behind El Niño by 4 months. By separating summer and winter seasons, the correlation is significantly improved. The summer NIE correlates positively with El Niño ($R = 0.62$), since tropical cyclones over the WNP tend to be stronger and longer-lived during the El Niño developing phase. The winter NIE correlates negatively with El Niño ($R = -0.65$), since the winter monsoon is weakened by the ENSO-related WNP anomalous anticyclone. This is the first time that interannual variability of NIE is studied by direct current velocity observations.

Plain Language Summary Interannual climate variability, especially El Niño-Southern Oscillation (ENSO), can trigger a series of flood, drought, and wildfires, resulting in a huge loss of people's property around the world. It has been demonstrated that ENSO can modulate large-scale oceanic and atmospheric processes, such as sea surface temperature, circulation, monsoon, tropical cyclones (TCs), etc. Near-inertial waves (NIWs) are ubiquitous in the upper ocean and usually contain the most energy of internal waves. Since NIWs are generated by time-varying wind stress, they could also be influenced by ENSO. Using current velocity observations from satellite-tracked surface drifter data set with hourly resolution, interannual variability of the surface mixed-layer near-inertial energy (NIE) is investigated. It is found that NIE in the western North Pacific (WNP) is indeed modulated by ENSO, with the monthly NIE lagging behind ENSO by 5 months. Since the monsoon reverses direction seasonally, summer and winter NIEs are discussed separately. The summer NIE is mainly generated by TCs while the winter NIE is mainly generated by winter monsoon, which are all tightly connected to and modulated by ENSO. Since NIWs play an important role in upper-ocean turbulent mixing and air-sea interaction, their interannual variations have important implications for the climate system.

1. Introduction

El Niño-Southern Oscillation (ENSO) is the most pronounced interannual climate variation on Earth. It has significant influences on human activities and many previous studies have focused on its modulation on the oceanic and atmospheric changes. Sea surface temperature (SST) anomalies (SSTA) in the tropical Pacific during El Niño could affect SSTA in the tropical Indian and Atlantic Oceans through Walker circulation (Chiang & Sobel, 2002; Latif & Barnett, 1995). El Niño could also affect the South China Sea (SCS) by inducing double-peak SSTA around February and August in the following El Niño year (Wang, Wang, et al., 2006). During the El Niño developing summer, the number of intense and recurve-northward tropical cyclones (TCs) significantly increases (Camargo & Sobel, 2005; Wang & Chan, 2002). Initiation of the western North Pacific anomalous anticyclone (WNPAC) over the Philippine Sea is induced by SST cooling that results from the combined effects of the mean northeast trade wind and equatorward wind anomalies caused by El Niño (Wang et al., 2000). The weakened northeast monsoon affected by the wintertime WNPAC leads to weaker Kuroshio Loop Current and upper Luzon Strait transport in the northern SCS (Chao et al., 1996; Sun et al., 2020; Wang, Fang, et al., 2006).

Small-scale processes could also be influenced by ENSO. For example, diapycnal mixing in the equatorial thermocline has been shown to be modulated by ENSO and is stronger during La Niña years (Richards et al., 2012). The northeast winter monsoon weakened by the El Niño-related WNPAC leads to reduced surface wave height in the SCS (Li et al., 2021). Due to the change of stratification, vertical structures of internal tides near Xisha Island in the SCS are modulated by ENSO (Zhai et al., 2020). Using stratification as a proxy, DeCarlo et al. (2015) showed that interannual variation of internal waves in the northern SCS is driven by intrusions of the Kuroshio and freshwater fluxes associated with ENSO.

Being disturbed by time-varying winds, the upper ocean continuously adjusts itself by radiating waves near the intrinsic frequency (i.e., f) of the rotating ocean, and thus near-inertial waves (NIWs) are generated. NIWs contain most of the high-frequency energy in the upper ocean and are important for turbulent mixing and air-sea interaction (Hummels et al., 2020; Jochum et al., 2013). Since the SCS and western North Pacific (WNP) region is influenced by the East Asian monsoon and TCs that are closely related to ENSO, what is the interannual variation of NIWs in this region? There has been no direct observation answering this question, and this provides direct motivation for the present work. Usually, the study of interannual variations of small-scale processes is difficult. On the one hand, in order to resolve small-scale process (e.g., NIWs), the time-resolution of observation must be high enough. On the other hand, in order to study interannual variations, the observation must contain at least several ENSO cycles. These requirements of high temporal resolution and long time series are contradicting and thus difficult to be satisfied simultaneously. Fortunately, satellite-tracked surface drifters providing hourly velocity records at 15-m depth for more than 30 years (Elipot et al., 2016) provide a unique opportunity for such an analysis. This surface drifter data set can be used to extract the mixed-layer near-inertial energy (NIE), which quantifies the intensity of NIWs.

Section 2 describes the data and methods used for the analysis. In Section 3, monthly NIE averaged in the study region is shown to correlate negatively (correlation coefficient $R = -0.44$) with ENSO with a time lag of 5 months. By separating summer and winter seasons, the summer and winter NIEs correlate positively ($R = 0.62$) and negatively ($R = -0.65$) with ENSO, respectively. The detailed physical mechanisms behind these correlations are identified. Finally, the conclusions are summarized in Section 4.

2. Data and Methods

2.1. Global Drifter Program Data Set

Satellite-tracked surface drifter data set from the Global Drifter Program (GDP) of National Oceanic and Atmospheric Administration (NOAA) provides horizontal current velocities and drifter positions at hourly intervals (Elipot et al., 2016). These drifters with drogues measure current velocity at 15-m depth, and the observations are more affected by the wind if the drogues are lost, that is, undrogued. For the SCS and WNP (108–135°E, 10–27°N), the drifter data span from October 2003 to March 2020. Drifters with lifetime shorter than 300 hr or breaking time longer than 10 hr are discarded. This results in 2,362,940 out of 2,576,285 velocity records being retained. The missing values are filled by linear interpolation. Although the spatial distribution of data is inhomogeneous in the study region (Figure 1a, see Figure S1 in Supporting Information S1 for the yearly spatial coverage of the drifters), most of the $0.5° \times 0.5°$ bins contain at least 1,000 velocity samples. Monthly distribution of the data (Figure 1b) indicates that most of the months contain at least 10,000 samples.

2.2. Current Velocity Correction and Wind Stress Fields

Since current velocities observed by drifters are influenced by winds (Niiler & Paduan, 1995), the 10-m wind velocities are used for current velocity correction. The wind data are from the European Centre for Medium-Range Weather Forecasts (ECMWF) Reanalysis V5 (ERA5), which have 1 hr temporal and 1/4° spatial resolutions and span from 1979 to 2020. The current velocity $\boldsymbol{U}_c$ is corrected as

$$\boldsymbol{U}_c = \boldsymbol{U}_0 - k \cdot \boldsymbol{U}_w, \tag{1}$$

where $\boldsymbol{U}_0$ is the measured velocity vector, $\boldsymbol{U}_w$ is the wind velocity vector linearly interpolated to the position and time of drifter observations, and k is a coefficient of correction. Following previous studies (Niiler et al., 1995; Pazan & Niiler, 2001), the coefficient is $k_d = 7 \times 10^{-4}$ when the drifter is drogued. When the drifter is undrogued,

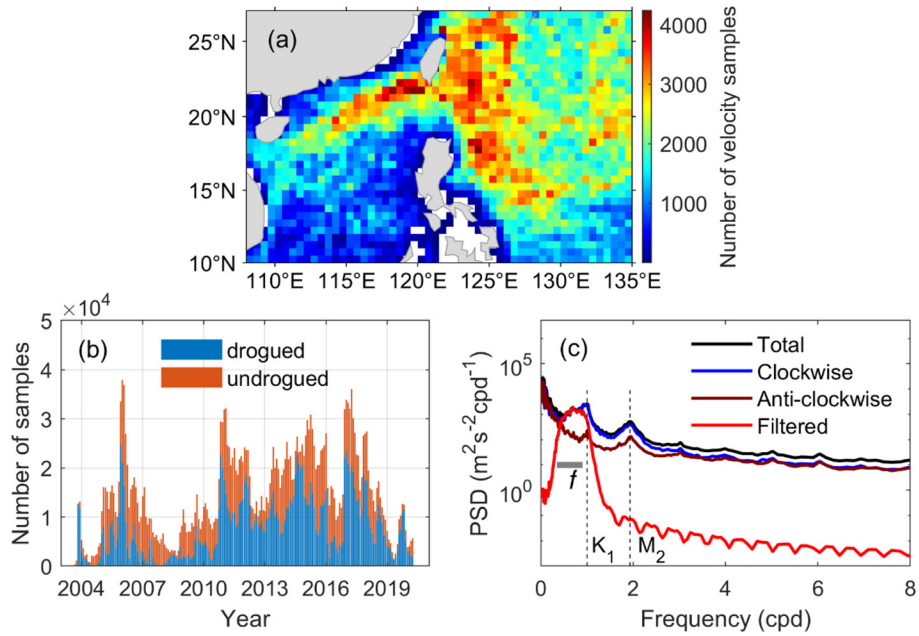

Figure 1. (a) Spatial distribution of the number of drifter velocity samples in 0.5° × 0.5° bins. (b) Monthly distribution of drifter velocity samples that are drogued and undrogued. (c) Averaged power spectral density (PSD) of velocity records (Total) and its clockwise and anti-clockwise components. The red line is PSD of the band-pass filtered velocity records. Vertical dotted lines indicate tidal frequencies. The horizontal bar marks the range of f in the region studied.

$$k_u = \left(\overline{u}_u - \overline{u}_d\right) / \overline{U}_w + k_d, \tag{2}$$

where $\overline{u}_d$ and $\overline{u}_u$ represent the downwind components of the drogued and undrogued drifter velocities, $\overline{U}_w$ is the amplitude of the wind speed, and the upper horizontal bar denotes spatially averaged value in a 4° × 4° spatial box (Laurindo et al., 2017).

To identify the dominant spatial mode of the wind field, Empirical Orthogonal Function (EOF) analysis is applied to the wind stress (WS) anomaly obtained by subtracting the climatological monthly-averaged WS field. The WS is calculated as

$$\mathrm{WS} = \sqrt{\tau_x^2 + \tau_y^2}, \tag{3}$$

where the zonal and meridional wind stress components are calculated as

$$(\tau_x, \tau_y) = \rho_a C_d \sqrt{u_{10}^2 + v_{10}^2}\,(u_{10}, v_{10}), \tag{4}$$

where $\rho_a = 1.3$ kg/m^3 is the air density, u_{10} and v_{10} are the 10-m wind velocities. The drag coefficient C_d follows the definition that can identify the strong wind stress by TCs (Oey et al., 2006). Near-inertial wind stress (IWS) is also used for analysis, which is calculated as

$$\mathrm{IWS} = \sqrt{\tau_{x,i}^2 + \tau_{y,i}^2}, \tag{5}$$

where $\tau_{x,i}$ and $\tau_{y,i}$ are obtained by band-pass filtering (0.6f–1.4f) τ_x and τ_y, respectively.

2.3. Surface Mixed-Layer NIE

The corrected drifter velocities are used for computing mixed-layer NIE. As the inertial frequency f varies along drifter trajectories, velocity records tracked by a drifter are broken into half-overlapping 300-hr segments as

in Liu et al. (2019). Then, f is set as the mean value over each segment and a band-pass filter (0.6f–1.4f, as in Chaigneau et al., 2008) is applied to extract the near-inertial velocities u_i and v_i. Averaged power spectral density (PSD) of all the corrected velocities (Total) and its clockwise and anti-clockwise components are shown in Figure 1c. Near the f range in the study region, the velocity vector mainly rotates clockwise with depth, corresponding to downward propagating wind-generated NIWs in the Northern Hemisphere. Diurnal and semi-diurnal tidal frequencies can also be discerned in the spectra. These features of the spectra are similar to those in Yu et al. (2019) that were also obtained from the GDP data set. Averaged PSD of the filtered near-inertial velocities is also shown (red line, see Figure S2 in the Supporting Information S1 for different filtering bands). It can be seen that the filtering adequately captures NIE in the study region. Finally, temperature data from World Ocean Atlas (WOA2018) are used for calculating the mixed-layer depth H, which is defined as the depth where the temperature is 0.5°C lower than the temperature of the surface 10-m layer (Monterey & Levitus, 1997). The mixed-layer NIE is then calculated as (Chaigneau et al., 2008).

$$\mathrm{NIE} = 0.5\rho_0 \left(u_i^2 + v_i^2\right) H, \tag{6}$$

where $\rho_0 = 1025\ \mathrm{kg/m^3}$ is a reference density of seawater.

2.4. Accumulated Cyclone Energy and Monsoon Indices

Since the SCS and WNP are influenced by TCs in summer, the accumulated cyclone energy (ACE) is adopted to quantify TC impacts (Bell et al., 2000):

$$\mathrm{ACE} = \sum {U_T}^2, \tag{7}$$

where U_T is the maximum sustained wind speed of an intense TC ($U_T \geq 17.2\ \mathrm{m/s}$) and the summation runs over all the individual TCs in the concerned period within the study region. The TC data are from Ying et al. (2014) and Lu et al. (2021).

To facilitate discussion of the forcing wind fields, different monsoon indices are used. The East Asia Winter Monsoon index (EAWM) is obtained by averaging the 1,000 hPa meridional wind over the SCS (7.5°N–20°N, 107.5°E−120°E) during December-January-February (DJF), which represents the intensity of the winter monsoon (Lu & Chan, 1999). The SCS Summer monsoon index (SCSSMI) is the same as EAWM, but for the summer monsoon during June-July-August (JJA).

3. Results and Discussion

3.1. Interannual Variation of NIE

Spatial distribution of the climatological mean mixed-layer NIE (see Figures S3 and S4 in Supporting Information S1 for potential biases due to the spatiotemporal coverage of the drifters) is shown in Figure 2a. The maximum mixed-layer NIE appears in the Luzon Strait, which agrees very well with the spatial pattern of the climatological mean WS in Figure 2b. This good agreement is consistent with the expectation that NIE in the surface mixed-layer is mainly generated by fluctuating WS (Alford et al., 2016). Since IWS is most efficient in resonantly generating NIWs (Chen et al., 2015; Crawford & Large, 1996), some studies used IWS as a proxy to identify interannual variations of wind power input into NIWs (Dippe et al., 2015; Rath et al., 2014). However, the spatial pattern of the climatological mean IWS (Figure 2c) agrees less well with the pattern of NIE (Figure 2a) than Figure 2b does. The temporal variations of NIE anomaly versus WS and IWS anomalies are shown in Figures 2d and 2e, respectively. The NIE anomaly correlates with the WS anomaly with a correlation coefficient $R = 0.43$, while it correlates with the IWS anomaly with $R = 0.62$. Thus, from the perspective of spatial variation, NIE in the study region correlates better with WS; while from the perspective of temporal variation, it correlates better with IWS. The reasons behind may deserve further study.

Interannual variation of the NIE anomaly smoothed with a 12-month sliding window is shown in Figure 2f. It correlates negatively ($R = -0.44$) with the Niño 3.4 index with a time lag of 5 months. This is mainly because the forcing WS correlates negatively ($R = -0.45$) with the Niño 3.4 index with a time lag of 4 months. This

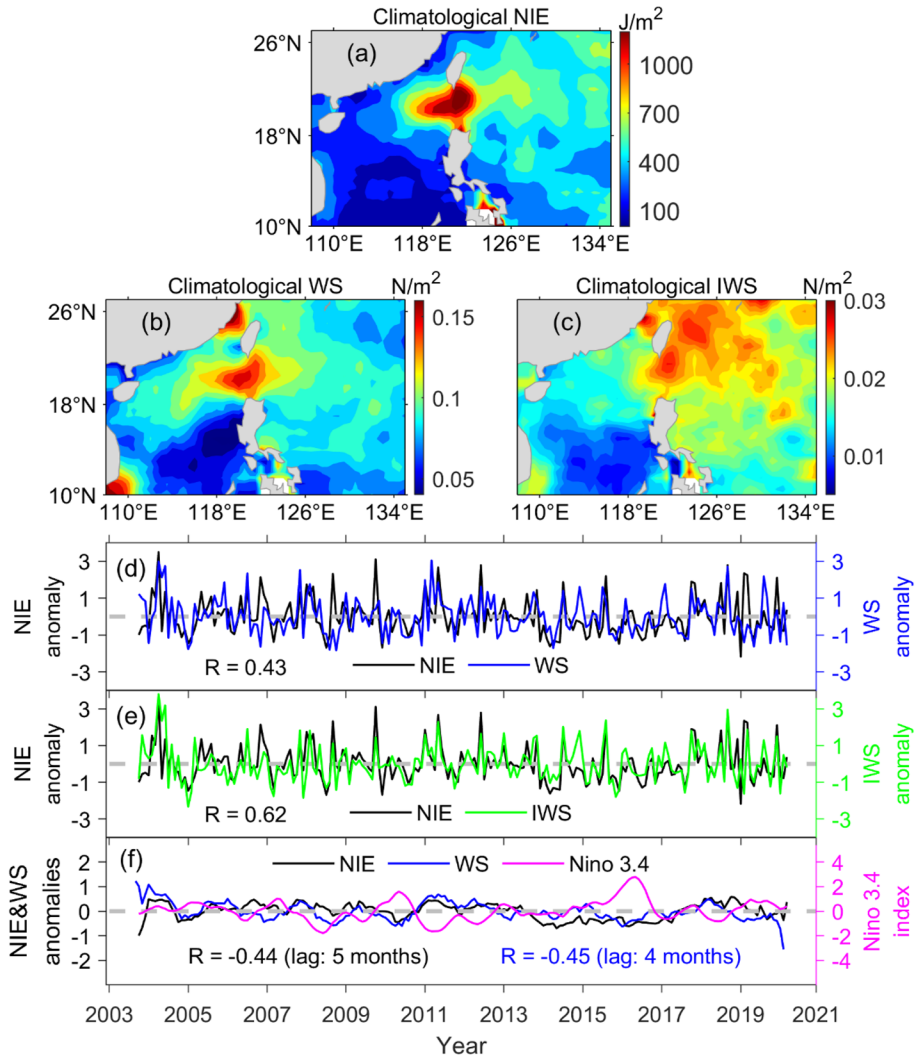

Figure 2. (a) Spatial distribution of the climatological mean mixed-layer NIE. (b) Spatial distribution of the climatological mean wind stress (WS) interpolated to the position and time of drifter observations. (c) The same as (b), but for near-inertial wind stress (IWS). (d) Mixed-layer NIE anomaly versus WS anomaly, with the correlation coefficient R indicated. (e) The same as (d), but for NIE and IWS anomalies. (f) Monthly WS and mixed-layer NIE anomalies smoothed with a 12-month sliding window, which achieve maximum correlation with the Niño 3.4 index with a time delay of 4 and 5 months, respectively. All the time series in (d–f) are standardized by dividing the anomalies by their corresponding standard deviations. All the correlation coefficients pass the *t*-test (95% confidence level).

suggests that there is a time lag of 1 month between NIE and WS. Note that the generation of NIWs in response to time-varying WS is very fast, usually within a few days. Thus, the 1-month time lag might be due to the monthly resolution of the time series.

To summarize, mixed-layer NIE and presumably turbulent mixing in the SCS and WNP are stronger after La Niña years and weaker after El Niño years. This is consistent with the short term in-situ observations that mixing in the western Pacific is modulated by ENSO and is stronger during La Niña years (Richards et al., 2012). Here, by using the GDP data set, we find that this is true for the whole SCS and WNP region and for a continuous long time series that contain several ENSO cycles. Also, we find a time lag of 5 months that cannot be discerned by the short term in-situ observations in specific months (Richards et al., 2012).

In the study region, the monsoon reverses direction seasonally and TCs mainly appear in summer. Thus, interannual variations of the summer and winter mixed-layer NIE will be separately discussed in the following sections.

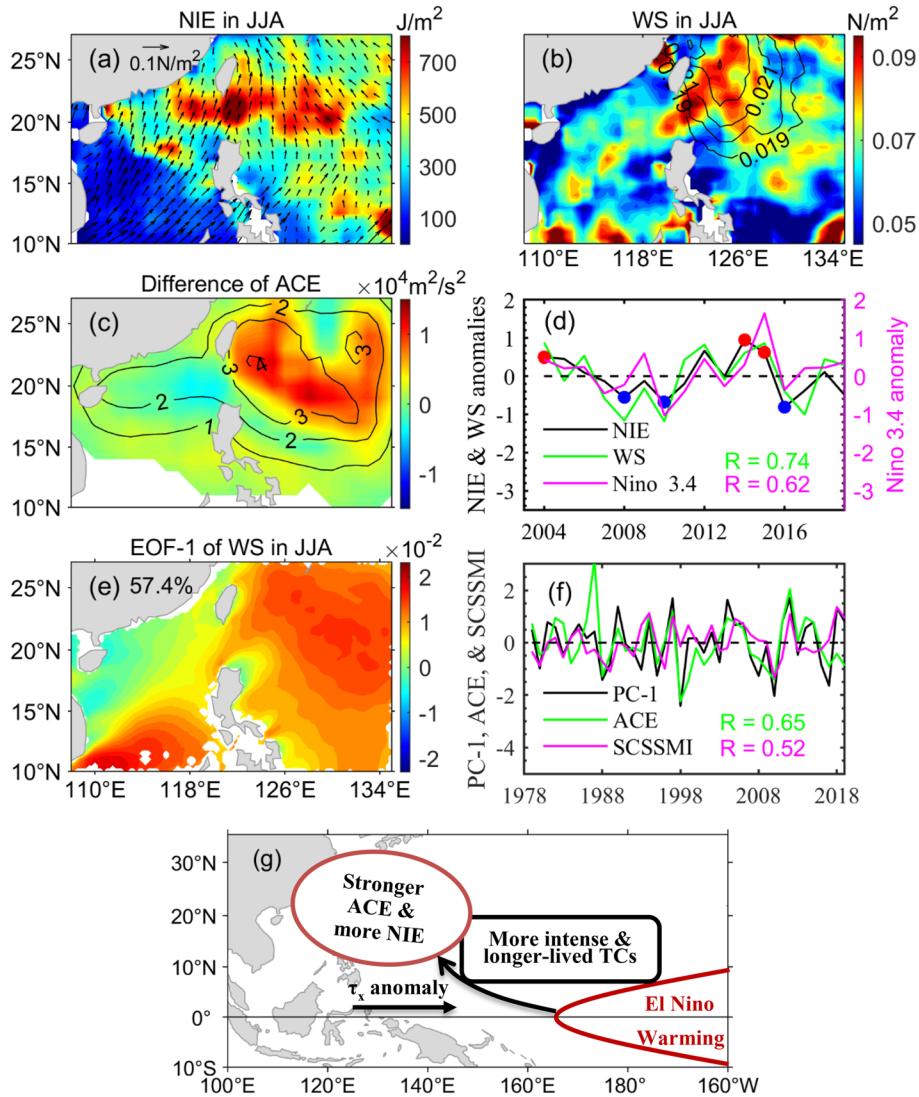

Figure 3. (a) The climatological mean mixed-layer NIE in summer (JJA). Arrows denote mean wind stress. (b) The same as (a), but for WS (color). Black lines are contours of climatological IWS, with contour spacing of 0.001 N/m^2. (c) Difference of the mean of ACE between El Niño and La Niña years (color). Black lines are contours (10^5 m^2/s^2) of the spatially averaged ACE during 1979–2019. (d) Summer NIE anomaly versus WS anomaly (green R) and the Niño 3.4 Index (magenta R). Red dots correspond to strong El Niño events while blue dots correspond to strong La Niña events. (e) Spatial pattern of EOF-1 of the WS anomalies. (f) The temporal coefficient of EOF-1 (PC-1; black line) versus the ACE index (green R) and the SCSSMI (magenta R). (g) A schematic of the mechanism responsible for the interannual variation of the summer mixed-layer NIE. All the time series are standardized as in Figure 2. All the correlation coefficients (R) pass the *t*-test (95% confidence level).

3.2. Interannual Variation of Summer NIE

Spatial distribution of the climatological mean mixed-layer NIE in summer (JJA) is shown in Figure 3a. It largely agrees with the spatial patterns of summer WS (color) and IWS (contours) in Figure 3b, except that there is high value of WS in the southern SCS due to the summer monsoon. Note that WS and IWS are interpolated to the position and time of drifter observations and thus the spatial patterns in Figure 3b also partly reflect the distribution of drifters in summer. The high WS and IWS near and to the east of the Luzon Strait are mainly generated by TCs. This is confirmed by the spatial pattern of ACE of TCs (contours in Figure 3c), which also agrees quite well with the NIE pattern in Figure 3a. This result thus suggests that the summer mixed-layer NIE in the study region is mainly due to the WNP TCs. The summer monsoon does not result in high NIE in the southern SCS, because it does not contain much IWS component that can effectively generate NIE (compare the color and contours in Figure 3b).

The summer NIE anomaly positively correlates with the WS anomaly with $R = 0.74$ (Figure 3d). It also positively correlates with the IWS anomaly ($R = 0.79$) and ACE index ($R = 0.8$) (not shown). As compared to the monthly NIE anomaly that correlates negatively with the Niño 3.4 index ($R = -0.44$) with a time lag of 5 months (Figure 2f), the summer NIE anomaly positively correlates with the Niño 3.4 index with $R = 0.62$. Three positive NIE anomalies (red dots) correspond well to the El Niño developing summer of 2004, 2014, and 2015, while three negative anomalies of NIE correspond well to the La Niña developing summer of 2008, 2010, and 2016.

To identify the region affected by ENSO, EOF analysis is applied to the WS anomaly. The first mode (EOF-1) explains 57.4% of the total variance (Figure 3e). This spatial pattern shows high value in the WNP, which corresponds well with the spatial pattern of ACE difference between El Niño and La Niña years (color in Figure 3c). It also shows high value in the southern SCS due to the summer monsoon. The principle component of EOF-1 of the WS anomaly (PC-1) shows a close relation with the ACE index, with $R = 0.65$ (Figure 3f). This suggests that TC activity in the WNP is significantly modulated by ENSO, with stronger ACE during El Niño developing years and weaker ACE during La Niña developing years. PC-1 of the WS anomaly has a weaker correlation with the SCSSMI ($R = 0.52$). However, since the summer monsoon does not have much IWS component (contours in Figure 3b) in the southern SCS, where indeed there is not much NIE (Figure 3a), the summer monsoon is not responsible for the generation of NIE. Note that the relatively less drifter observations in the southern SCS (Figure 1a) might also lead to the absence of high NIE there.

The modulation of ENSO on summer NIE is summarized in Figure 3g. During El Niño development in summer, SST warming over the equatorial eastern-central Pacific intensifies convective heating around 180°, inducing westerly anomalies to the west of the warming region that are the precondition of spinning up TCs. The low-level shear vorticity of the background wind is intensified by the westerly burst, leading to more TCs generated in the tropical Pacific (Wang & Chan, 2002). These more intense and longer-lived TCs tend to recurve northward (Camargo & Sobel, 2005; Wang & Chan, 2002), inducing stronger ACE and thus generating higher NIE in the WNP.

3.3. Interannual Variation of Winter NIE

Spatial distribution of the climatological mean mixed-layer NIE in winter (DJF) is shown in Figure 4a. Similar to that in Figure 2a, strong NIE appears in the Luzon Strait, which is largely consistent with the patterns of WS (color) and IWS (contours) in Figure 4b. Strong orographic wind jets over the Luzon Strait (Wang et al., 2008) generate strong WS and thus NIE in winter. The NIE anomaly correlates positively ($R = 0.52$) with the WS anomaly and it correlates negatively ($R = -0.65$) with the Niño 3.4 index (Figure 4c). Four negative anomalies of NIE correspond well to the El Niño years of 2004–2005, 2009–2010, 2014–2015, and 2015–2016 (red dots in Figure 4c), while four positive anomalies of NIE correspond well to the La Niña years of 2005–2006, 2007–2008, 2010–2011, and 2017–2018 (blue dots in Figure 4c). This suggests that winter mixed-layer NIE is also modulated by ENSO, with stronger NIE during La Niña winters and weaker NIE during El Niño winters.

EOF-1 of the winter WS anomaly shows high values in the SCS and WNP, which explains 63.9% of the total variance (Figure 4d). This spatial pattern agrees very well with the difference of WS between La Niña and El Niño years (Figure 4e), revealing that ENSO plays a key role in modulating interannual variation of winter WS in the study region. PC-1 shows a close relation with the EAWM index, with $R = -0.76$, indicating that the wind field is mainly affected by winter monsoon (Figure 4f).

The modulation of ENSO on winter NIE is summarized in Figure 4g. During El Niño years, surface warming over the equatorial eastern-central Pacific intensifies convective heating around 180°, inducing a cyclone to the northwest of the warming region (Wang et al., 2000). Surface cooling to the west of the warming region, generated by the strong wind due to a combination of the cyclone and trade wind, excites an El Niño-induced WNPAC (Wang et al., 2000). Such a WNPAC weakens the northeasterly winter monsoon, leading to weaker WS and smaller mixed-layer NIE in the study region. Consistent with previous studies (Li et al., 2021; Xu et al., 2019; Yuan & Yang, 2012), composite wind anomalies of strong El Niño events (not shown) exhibit an obvious anomalous cyclone to the northwest of the warming region and a WNPAC around the Philippine Sea.

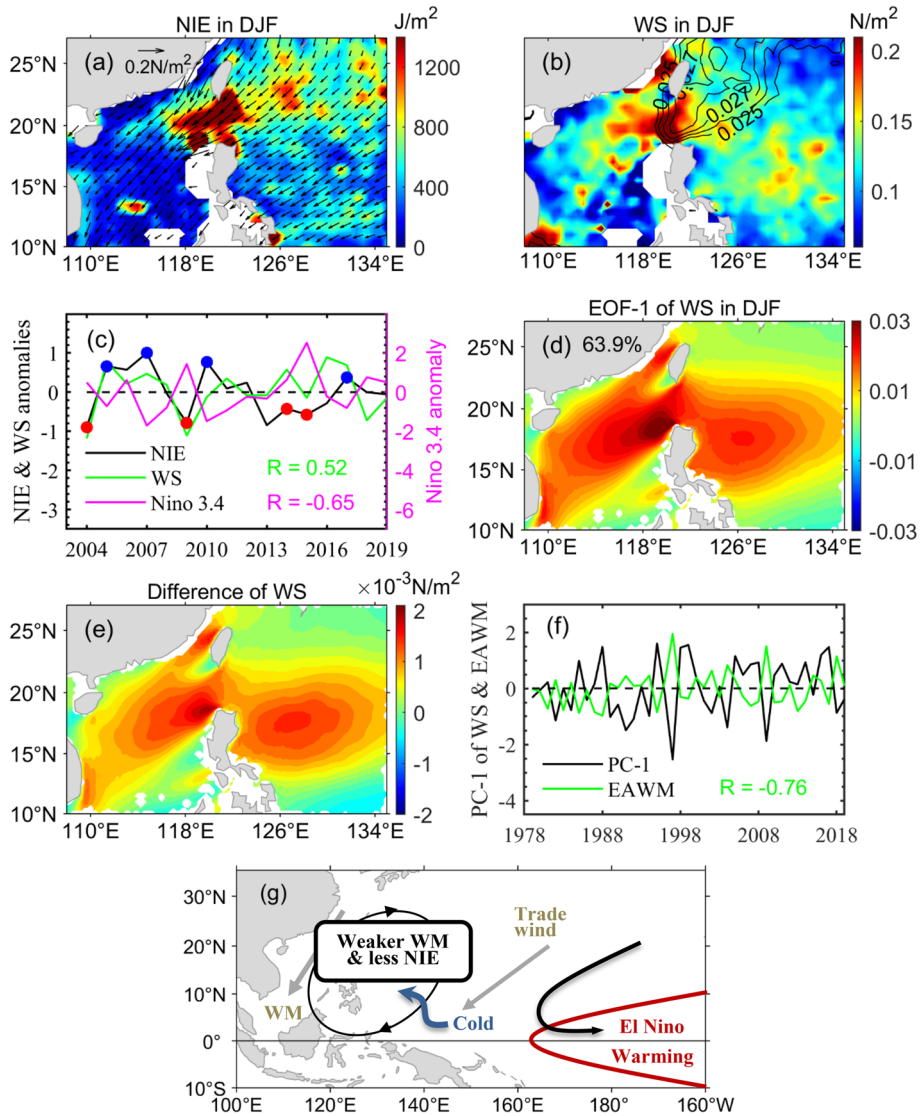

Figure 4. (a) The climatological mean NIE in winter (DJF). Arrows denote mean wind stress. (b) The same as (a), but for WS (color). Black lines are contours of climatological IWS. (c) The winter NIE anomaly versus WS anomaly (green R) and the Niño 3.4 index (magenta R). Red dots correspond to strong El Niño events while blue dots correspond to strong La Niña events. (d) Spatial pattern of EOF-1 of the WS anomalies. (e) The difference of WS between La Niña and El Niño years. (f) PC-1 versus the East Asia Winter Monsoon index (EAWM). (g) A schematic of the mechanism responsible for the interannual variation of the winter NIE, referring to Wang et al. (2000). All the time series are standardized as in Figure 2.

4. Conclusion

Interannual variations of surface mixed-layer NIE extracted from satellite-tracked surface drifter data set with hourly resolution in the SCS and WNP are investigated in the present study. The monthly NIE correlates negatively ($R = -0.44$) with the Niño 3.4 index with a time lag of 5 months, which is primarily due to the delayed wind-response to ENSO events in the study region. By separating summer and winter seasons, it is found that during the El Niño developing summer, NIE correlates positively ($R = 0.62$) with the Niño 3.4 index due to the stronger and longer-lived TCs in the WNP. During the El Niño mature phase in winter, NIE correlates negatively ($R = -0.65$) with the Niño 3.4 index due to the weakened winter monsoon by the El Niño-induced WNPAC. To the authors' knowledge, this is the first time that interannual variations of surface mixed-layer NIE (thus the intensity of NIWs) are investigated by direct current velocity observations. Since NIWs usually occupy the most kinetic energy of internal waves and play an important role in turbulent mixing, air-sea interaction, etc., their interannual variations may be important for the climate system.

Data Availability Statement

The drifter data are available at https://www.aoml.noaa.gov/phod/gdp/hourly_data.php. The WOA2018 temperature data are available at https://www.ncei.noaa.gov/access/world-ocean-atlas-2018/bin/woa18.pl. The TC data are available at https://tcdata.typhoon.org.cn/zjljsjj_zlhq.html. The ERA5 wind data are available at https://cds.climate.copernicus.eu/cdsapp%23%21/dataset/reanalysis%2Dera5%2Dsingle%2Dlevels%3Ftab%3Dform.

Acknowledgments
This work was jointly supported by the National Natural Science Foundation of China (Nos. 42130404, 91858201, 42192564, 41622601, 42176025, 42276022, and 42206012), the Frontier Science Key Research Program of CAS (QYZDJ-SSW-DQC034), No. GML2019ZD0304 from Southern Marine Science and Engineering Guangdong Laboratory (Guangzhou), LTO Independent Research Program (LTOZZ2001 and LTOZZ2205), No. ISEE2021PY01 from CAS, and the Science and Technology Projects of Guangzhou (No. 202102020897).

References

Alford, M. H., MacKinnon, J. A., Simmons, H. L., & Nash, J. D. (2016). Near-inertial internal gravity waves in the ocean. *Annual Review of Marine Science*, *8*(1), 95–123. https://doi.org/10.1146/annurev-marine-010814-015746

Bell, G. D., Halpert, M. S., Schnell, R., Higgins, W., Lawrimore, J., Kousky, V. E., et al. (2000). Climate assessment for 1999. *Bulletin of the American Meteorological Society*, *81*(6), S1–S50. https://doi.org/10.1175/1520-0477(2000)81[s1:CAF]2.0.CO;2

Camargo, S. J., & Sobel, A. H. (2005). Western North Pacific tropical cyclone intensity and ENSO. *Journal of Climate*, *18*(15), 2996–3006. https://doi.org/10.1175/JCLI3457.1

Chaigneau, A., Pizarro, O., & Rojas, W. (2008). Global climatology of near-inertial current characteristics from Lagrangian observations. *Geophysical Research Letters*, *35*(13), L13603. https://doi.org/10.1029/2008GL034060

Chao, S.-Y., Shaw, P.-T., & Wu, S. Y. (1996). El Niño modulation of the South China sea circulation. *Progress in Oceanography*, *38*(1), 51–93. https://doi.org/10.1016/S0079-6611(96)00010-9

Chen, S. L., Polton, J. A., Hu, J. Y., & Xing, J. X. (2015). Local inertial oscillations in the surface ocean generated by time-varying winds. *Ocean Dynamics*, *65*(12), 1633–1641. https://doi.org/10.1007/s10236-015-0899-6

Chiang, J. C. H., & Sobel, A. H. (2002). Tropical tropospheric temperature variations caused by ENSO and their influence on the remote tropical climate. *Journal of Climate*, *15*(18), 2616–2631. https://doi.org/10.1175/1520-0442(2002)015<2616:TTTVCB>2.0.CO;2

Crawford, G. B., & Large, W. G. (1996). A numerical investigation of resonant inertial response of the ocean to wind forcing. *Journal of Physical Oceanography*, *26*(6), 873–891. https://doi.org/10.1175/1520-0485(1996)026<0873:ANIORI>2.0.CO;2

DeCarlo, T. M., Karnauskas, K. B., Davis, K. A., & Wong, G. T. F. (2015). Climate modulates internal wave activity in the Northern South China Sea. *Geophysical Research Letters*, *42*(3), 831–838. https://doi.org/10.1002/2014GL062522

Dippe, T., Zhai, X. M., Greatbatch, R., & Rath, W. (2015). Interannual variability of wind power input to near-inertial motions in the North Atlantic. *Ocean Dynamics*, *65*(6), 859–875. https://doi.org/10.1007/s10236-015-0834-x

Elipot, S., Lumpkin, R., Perez, R. C., Lilly, J. M., Early, J. J., & Sykulski, A. M. (2016). A global surface drifter data set at hourly resolution. *Journal of Geophysical Research: Oceans*, *121*(5), 2937–2966. https://doi.org/10.1002/2016JC011716

Hummels, R., Dengler, M., Rath, W., Foltz, G. R., Schutte, F., Fischer, T., & Brandt, P. (2020). Surface cooling caused by rare but intense near-inertial wave induced mixing in the tropical Atlantic. *Nature Communications*, *11*(1), 3829. https://doi.org/10.1038/s41467-020-17601-x

Jochum, M., Briegleb, B. P., Danabasoglu, G., Large, W. G., Norton, N. J., Jayne, S. R., et al. (2013). The impact of oceanic near-inertial waves on climate. *Journal of Climate*, *26*(9), 2833–2844. https://doi.org/10.1175/JCLI-D-12-00181.1

Latif, M., & Barnett, T. P. (1995). Interaction of the tropical oceans. *Journal of Climate*, *8*(4), 952–964. https://doi.org/10.1175/1520-0442(1995)008<0952:IOTTO>2.0.CO;2

Laurindo, L. C., Mariano, A. J., & Lumpkin, R. (2017). An improved near-surface velocity climatology for the global ocean from drifter observations. *Deep-Sea Research Part I Oceanographic Research Papers*, *124*, 73–92. https://doi.org/10.1016/j.dsr.2017.04.009

Li, S. T., Li, Y. N., Peng, S. Q., & Qi, Z. H. (2021). The inter-annual variations of the significant wave height in the Western North Pacific and South China Sea region. *Climate Dynamics*, *56*(9–10), 3065–3080. https://doi.org/10.1007/s00382-021-05636-9

Liu, Y. Z., Jing, Z., & Wu, L. X. (2019). Wind power on oceanic near-inertial oscillations in the global ocean estimated from surface drifters. *Geophysical Research Letters*, *46*(5), 2647–2653. https://doi.org/10.1029/2018GL081712

Lu, E., & Chan, J. C. L. (1999). A unified monsoon index for South China. *Journal of Climate*, *12*(8), 2375–2385. https://doi.org/10.1175/1520-0442(1999)012<2375:AUMIFS>2.0.CO;2

Lu, X. Q., Yu, H., Ying, M., Zhao, B. K., Zhang, S., Lin, L. M., et al. (2021). Western North Pacific tropical cyclone database created by the China Meteorological Administration. *Advances in Atmospheric Sciences*, *38*(4), 690–699. https://doi.org/10.1007/s00376-020-0211-7

Monterey, G. I., & Levitus, S. (1997). Seasonal variability of mixed layer depth for the world ocean. *NOAA Atlas NESDIS* (Vol. 14, p. 100). U.S. Government. Printing Office.

Niiler, P. P., & Paduan, J. D. (1995). Wind-driven motions in the Northeast Pacific as measured by Lagrangian drifters. *Journal of Physical Oceanography*, *25*(11), 2819–2830. https://doi.org/10.1175/1520-0485(1995)025<2819:WDMITN>2.0.CO;2

Niiler, P. P., Sybrandy, A. S., Bi, K. N., Poulain, P. M., & Bitterman, D. (1995). Measurements of the water-following capability of holey-sock and TRISTAR drifters. *Deep-Sea Research Part I Oceanographic Research Papers*, *42*(11–12), 1951–1964. https://doi.org/10.1016/0967-0637(95)00076-3

Oey, L. Y., Ezer, T., Wang, D. P., Fan, S. J., & Yin, X. Q. (2006). Loop current warming by Hurricane Wilma. *Geophysical Research Letters*, *33*(8), L08613. https://doi.org/10.1029/2006GL025873

Pazan, S. E., & Niiler, P. P. (2001). Recovery of near-surface velocity from undrogued drifters. *Journal of Atmospheric and Oceanic Technology*, *18*(3), 476–489. https://doi.org/10.1175/1520-0426(2001)018<0476:RONSVF>2.0.CO;2

Rath, W., Greatbatch, R. J., & Zhai, X. M. (2014). On the spatial and temporal distribution of near-inertial energy in the Southern Ocean. *Journal of Geophysical Research: Oceans*, *119*(1), 359–376. https://doi.org/10.1002/2013JC009246

Richards, K. J., Kashino, Y., Natarov, A., & Firing, E. (2012). Mixing in the western equatorial Pacific and its modulation by ENSO. *Geophysical Research Letters*, *39*(2), L02604. https://doi.org/10.1029/2011GL050439

Sun, Z. B., Zhang, Z. W., Qiu, B., Zhang, X. C., Zhou, C., Huang, X. D., et al. (2020). Three-dimensional structure and interannual variability of the Kuroshio Loop current in the northeastern South China Sea. *Journal of Physical Oceanography*, *50*(9), 2437–2455. https://doi.org/10.1175/JPO-D-20-0058.1

Wang, B., & Chan, J. C. L. (2002). How strong ENSO events affect tropical storm activity over the western North Pacific. *Journal of Climate*, *15*(13), 1643–1658. https://doi.org/10.1175/1520-0442(2002)015<1643:HSEEAT>2.0.CO;2

Wang, B., Wu, R. G., & Fu, X. H. (2000). Pacific-East Asian teleconnection: How does ENSO affect East Asian climate? *Journal of Climate*, *13*(9), 1517–1536. https://doi.org/10.1175/1520-0442(2000)013<1517:PEATHD>2.0.CO;2

Wang, C., Wang, W., Wang, D., & Wang, Q. (2006). Interannual variability of the South China Sea associated with El Niño. *Journal of Geophysical Research*, *111*(C3), C03023. https://doi.org/10.1029/2005JC003333

Wang, G. H., Chen, D., & Su, J. L. (2008). Winter eddy Genesis in the eastern South China Sea due to orographic wind jets. *Journal of Physical Oceanography*, *38*(3), 726–732. https://doi.org/10.1175/2007JPO3868.1

Wang, Y. G., Fang, G. H., Wei, Z. X., Qiao, F. L., & Chen, H. Y. (2006). Interannual variation of the South China Sea circulation and its relation to El Nino, as seen from a variable grid global ocean model. *Journal of Geophysical Research*, *111*(C11), C11S14. https://doi.org/10.1029/2005JC003269

Xu, K., Huang, Q. L., Tam, C. Y., Wang, W. Q., Chen, S., & Zhu, C. W. (2019). Roles of tropical SST patterns during two types of ENSO in modulating wintertime rainfall over southern China. *Climate Dynamics*, *52*(1–2), 523–538. https://doi.org/10.1007/s00382-018-4170-y

Ying, M., Zhang, W., Yu, H., Lu, X. Q., Feng, J. X., Fan, Y. X., et al. (2014). An overview of the China Meteorological Administration tropical cyclone database. *Journal of Atmospheric and Oceanic Technology*, *31*(2), 287–301. https://doi.org/10.1175/JTECH-D-12-00119.1

Yu, X. L., Ponte, A. L., Elipot, S., Menemenlis, D., Zaron, E. D., & Abernathey, R. (2019). Surface kinetic energy distributions in the global oceans from a high-resolution numerical model and surface drifter observations. *Geophysical Research Letters*, *46*(16), 9757–9766. https://doi.org/10.1029/2019GL083074

Yuan, Y., & Yang, S. (2012). Impacts of different types of El Nino on the East Asian climate: Focus on ENSO cycles. *Journal of Climate*, *25*(21), 7702–7722. https://doi.org/10.1175/JCLI-D-11-00576.1

Zhai, R. W., Chen, G. Y., Liang, C. R., Shang, X. D., & Xie, J. S. (2020). The influence of ENSO on the structure of internal tides in the Xisha area. *Journal of Geophysical Research: Oceans*, *125*(3), e2019JC015405. https://doi.org/10.1029/2019JC015405